Estimation Method for Residual Sodium Amount on Unloaded Dummy Fuel Assembly

Munemichi Kawaguchi[a]*, Yasushi Hirakawa[a], Yusuke Sugita[a] and Yutaka Yamaguchi[a]

[a]*Japan Atomic Energy Agency, Tsuruga, Fukui, Japan*

*Corresponding author

Current affiliation	Hokkaido University
Email	kawaguchi.munemichi@eng.hokudai.ac.jp
Present address	Kita-13, Nishi-8, Kita-ku, Sapporo, Hokkaido 060-8628, Japan
ORCiDs	0000-0002-4038-565X

*Current affiliation	Hokkaido University
*Present address	Kita-13, Nishi-8, Kita-ku, Sapporo, Hokkaido 060-8628, Japan

Estimation Method for Residual Sodium Amount on Unloaded Dummy Fuel Assembly

This study has researched an estimation method for amounts of residual sodium film and sodium lumps on dummy fuel pins in Monju by the fundamental experiments and demonstration experiments. The residual sodium amounts on the pin surface were measured using the three-type test specimens: (a) single pin, (b) 7-pin assembly, and (c) 169-pin assembly. The single pin and 7-pin assembly experiments revealed that the withdrawal speed of the pins and improvement of the sodium wetting increased drastically the residual sodium amounts. Furthermore, the 169-pin assembly experiments measured the practical amounts of the residual sodium in the Monju dummy fuel assembly and demonstrated a sodium draining behavior through small gaps between the pins.

The estimation method includes four models such as a viscosity flow model, Landau–Levich–Derjaguin (LLD) model, an empirical equation related to the Bretherton model, and a capillary force model in a tube. These calculation results were comparable to the residual sodium amounts obtained by the experiments. In the tests of improving the sodium wetting, the amounts of the residual sodium on the test specimen were close to 1.4 times larger than those of the thin sodium film estimated by the LLD model. The increased amount of residual sodium by improving the sodium wetting was explained by the ratio of the adhesion energy ($\gamma_{SO} - \gamma_{SL}$).

Keywords: sodium cooled fast reactor; dummy fuel assembly; residual sodium; wet cleaning process; capillary.

I. Introduction

In the fuel cleaning facility of the Japanese prototype fast breeder reactor, Monju, a wet cleaning system has been adopted[1]. When the spent fuel assembly was unloaded, a small amount of residual radioactive primary-circuit sodium was attached to the assembly. The liquid sodium easily remains due to the dense

structures in the inside of the wrapper tube. **Figure 1** depicts an outline of the Monju fuel assembly, which consists of many fuel elements and structures in a hexagonal wrapper tube[2]. The fuel elements are filled with the fuel pellets in a stainless-steel cladding tube, sealed at the top and bottom ends. Wire spacers are wound around the cladding tubes of a driver fuel pin, which stand by themselves in the wrapper tube. The liquid sodium easily remains due to the dense structures in the inside of the wrapper tube. However, the gap between the pins in the dummy fuel assembly is smaller than in the driver fuel assembly because the wire spacers were removed from the dummy fuel pins to simplify the core structure. The cross-sectional areas of the gap (S) were close to 7.84 mm^2 for the driver fuel pins and 3.13 mm^2 for the dummy fuel pins.

< Figure 1 >

In the Monju fuel cleaning facility, the residual sodium was first reacted with a mixture gas of argon and steam to remove roughly the radioactive primary-circuit sodium from the assembly. Then, the assembly was rinsed well with distilled water as the second cleaning process. In July 2021, the wet cleaning process of the 406 fuel assemblies has been carried out in the 530 assemblies unloaded from both the reactor vessel and the ex-vessel fuel storage tank in Monju[3]. The residual sodium amounts of the rinsed fuel assemblies were evaluated at less than 270 g per unit assembly by measuring the amounts of hydrogen gas generated from the sodium-water reaction. These sodium amounts include the total residual sodium amounts of both the fuel pin surface (m_{Driver}) and the assembly structures (M_{Driver}) such as a handling head, a wrapper tube, and the entrance nozzle, as seen in Figure 1. The residual sodium amount of the dummy fuel assembly except for the pins (M_{Dummy}) should be comparable to that of the driver fuel assembly except for the pins ($M_{Driver} = M_{Dummy}$) because the same device was used for the dummy fuel assembly. However, in the residual sodium amounts of the dummy fuel pins (m_{Driver}), a larger amount of liquid sodium would be deposited, or the liquid sodium might not drain through a gap between the dummy fuel pins due to the small gap area. Then, the large amount of residual sodium would lead to an unsafe decommissioning process, e. g., the residual sodium amounts exceed the capacity of the fuel cleaning facility. In this study, we investigated the residual

sodium amounts (m_{Dummy}) deposited on the dummy fuel pins during the withdrawal of the pins from the sodium pool.

The liquid behavior deposited on the solid surface has been researched extensively as hydrodynamics and wetting problems, e. g., dip-coating technology[4–5]. The studies have found mechanisms for liquid film formation on the solid surface and universal formulae for the liquid film thickness. In addition, some experimental data on residual sodium amounts of the fuel pins and various shape specimens have been reported[6–7]. Also, some researchers have revealed wetting phenomena between liquid sodium and solid stainless steel surface[8–13]. However, from practical and quantitative viewpoints, they are not sufficient for the assessment of the residual sodium amount deposited on the Monju dummy fuel assembly. This is because quantitative data on residual sodium amounts in the current Monju dummy fuel pins without the wire spacer haven't been obtained experimentally. In addition, it is unknown how the improvement of wetting affects the residual sodium amount.

This study measured amounts of sodium film deposited on the dummy fuel pin surface and sodium lumps at the bottom of the dummy fuel pins and compared the experiment and the calculation results using the estimation method. The estimation method focuses on the amount of residual sodium on the dummy fuel pins without wire spacers, because the amount of residual sodium on the fuel assembly is equivalent to that of the driver fuel assembly ($M_{Driver} = M_{Dummy}$). Based on the characteristics of the residual sodium on the dummy fuel pin, such as the thin sodium film forms at the upper of the dummy fuel pin and the sodium lump deposits at the bottom of the fuel pin, the estimation method was to combine the representative four equations of viscosity flow model, LLD model, empirical equation related to Bretherton model, and capillary force model in a tube. Furthermore, we demonstrated experimentally the sodium draining behavior through the gaps between the dummy fuel pins to realize the wet cleaning for the dummy fuel assembly in the Monju facility.

II. Experiment

II.A. Test apparatus and procedure

Figure 2 depicts an overview of two types of test apparatus for (a) single pin or 7-pin assembly and for (b) 169-pin assembly: a small test specimen of a single pin and 7-pin assembly were arranged to obtain fundamental experimental data, such as the amounts of residual sodium film on the outer surface of the pin and sodium lump at the bottom gap between the several pins. In experiment (a), the sodium of Métaux Spéciaux with a stated purity of 99.98% in the cylindrical stainless-steel vessel (diameter: 0.0535 m, height: 0.21 m) was heated at 200°C or 350°C with the mantle heater in a glovebox. The test specimen was immersed in the liquid sodium and evacuated by a pump to exclude the gas attached on the surface of the test specimen. Therefore, the gas among the pins was replaced by liquid sodium. The sodium temperature was set at 200°C, which was the same as the Monju condition. The test specimen was extracted from the liquid sodium at a low withdrawal speed of approximately 0.004 m/s by the electric lab jacks and at a high withdrawal speed of more than 0.1 m/s by hand to obtain the fundamental experimental data. Experiment (b) used the sodium tank (diameter: 0.3 m, height: 0.4 m) in the same glovebox system, which was combined with the sodium loop apparatus. This experimental apparatus is the glove box for maintenance technology tests of Japan Atomic Energy Agency[14]. In this sodium tank, a large test specimen of 169-pin assembly without/with the wrapper tube was experimented with to quantify the residual sodium amount on the unloaded 169 dummy fuel pins and to demonstrate the sodium draining behavior through the gaps between the dummy fuel pins. The gap length between the pins is close to 0.1 mm in width. The 169-pin assembly was immersed into the liquid sodium of 200°C in the sodium tank, and the cover gas in the sodium tank was evacuated by the pump. Then, the 169-pin assembly was extracted at the withdrawal speed of 0.1 m/s. In the immerse and extract operations of the 169-pin assembly, we used the electric winch (BMS-360H10, TOYO KOKEN K. K.). The withdrawal speed was fixed at 0.1 m/s, which is the same as Monju. The sodium draining behavior with the 169-pin assembly during withdrawing was recorded visually with a home-use video camera.

< Figure 2 >

These procedures were performed in an inert Ar atmosphere of the glovebox system, where the oxygen concentration and the dew point were kept at less than 1 ppm and less than –76°C, respectively. The atmosphere temperature in the glovebox was measured at approximately 20°C for (a) single pin or 7-pin assembly and at approximately 50°C for (b) 169-pin assembly. The cover gas temperatures were comparable to the atmospheric temperatures in the glove box.

II.B. Test specimen

Figure 3 depicts the four types of test specimens: (a) single pin, (b) 7-pin assembly, and (c)–(d) 169-pin assembly without/with a wrapper tube. The pins and assembly were simulated as the dummy fuel assembly of Monju: the pins were designed at 7.8 mm in diameter. The pins were arranged in a hexagon with a gap of 0.1 mm between the pins. The test specimens were made of the same material as the Monju dummy fuel pin of type-304 stainless steel. **Table 1** shows the components of the Monju dummy fuel pin. The manufacturing conditions such as the diameter and surface roughness are the same as Monju. However, the heights of the pins were 150 mm for (a) single pin and (b) 7-pin assembly for the handling of the experiments. They were 300 mm for (c)–(d) 169-pin assembly. In (c)–(d) 169-pin assembly, the number of pins per unit assembly was the same as 169 pins of the Monju dummy fuel assembly. Furthermore, (d) 169-pin assembly simulated the sodium flow channel of the Monju dummy fuel assembly by fixing the pins at a locking plate at the bottom of the assembly. The drain ports were prepared for liquid sodium draining from the wrapper tube. The size of the drain ports was approximately 30 mm^{H} × 20 mm^{L} × 3 mm^{W}. All the test specimens were reused after rinsing very well with alcohol and distilled water.

< Figure 3 >

< Table 1 >

II.C. Post-test analysis

(1) Post-test chemical analysis

After the tests, we rinsed the post-test pins with industrial alcohol containing 85.6% ethanol, 9.5% normal propanol, 4.9% isopropyl alcohol, and a little water. To evaluate quantitatively the amount of residual sodium, we performed the post-test chemical analysis for the rinsed alcohol solution. First, the rinsed alcohol solution was evaporated to dryness. The post-test chemical analysis sample was prepared by diluting it with distilled water. Second, the amounts of sodium in the blank industrial alcohol and the post-test chemical analysis sample of the rinsed alcohol solution were quantitated by Flame Atomic Absorption Spectrometry (AAS)[15]. The AAS can determine the concentration of a metallic element in solution as based on absorption of light by free metallic ions. The AAS instrument used ZA3300 (Hitachi High-Tech Science Corporation)[16]. We evaluated the concentration of sodium from the area of the signal intensity in the spectra using the three-point calibration curve method (0, 10, and 20 mg/l). The analyzed values were taken as an average of the three-time analyzed results. The minimum limits of detection were less than 1 ppm. The measured values were more than 10 times higher than the blank industrial alcohol in sodium concentration. The detection ability was sufficiency.

(2) Image analysis

The experimental withdrawal speeds of the pins in Run 1-1 to 1-8 were evaluated by the image analyses of the recorded movies because it is essential parameters for the liquid sodium film formation. In the image analysis, we first translated the movies to the still images at intervals of less than 0.2 s. Next, the pull-out length of the pins was evaluated by using a generic image analysis software (Ryushi-kaiseki ver. 3.5, Nippon steel). We used the raw still images that haven't never processed such as an image filtering. Here, the pull-out lengths were close to 40 mm for the small withdrawal speed and close to 170 mm for the large withdrawal speed as based on the pin diameter, respectively. Then, we calculated the withdrawal speeds of the pins in Run 1-1 to 1-8 using the pull-out lengths and

times. In Run 1-9 to 2-3, the withdrawal speeds weren't evaluated since the electric winch was a fixed withdrawal speed (0.1 m/s).

II.D. Test conditions

Table 2 shows the experimental conditions: a series of Run 1-1 to 1-11 targets to quantify the residual sodium amounts, which depend on the withdrawal speed and the sodium wetting. In Run 1-1 to 1-4, the residual sodium amounts deposited on the surface of the single pin were quantitatively measured. The withdrawal speeds of Run 1-1 and 1-3 were set as close to 0.004 m/s, and those of Run 1-2 and 1-4 were set as more than 0.1 m/s, respectively. Table 2 shows the withdrawal speeds obtained from the image analyses. They were 0.004 ± 0.000 m/s in Run 1-1 and 1-3 and 0.170 ± 0.013 m/s in Run 1-2 and 0.189 ± 0.003 m/s in Run 1-4. At the withdrawal speed of 0.004 m/s, the liquid sodium on the pin surface flowed slowly along the pin's length direction due to the gravitation. It simulates a viscous flow regime for the unloaded pin. On the other hand, at the withdrawal speed of more than 0.1 m/s, the liquid sodium depended on the competition between the gravitation and surface tension around the sodium pool surface. It would be an intermediate condition between a viscous flow regime and a capillary flow regime. Furthermore, in Run 1-3 to 1-4, the test specimens were immersed in the liquid sodium of 350°C for two hours prior to unloading (preheating) to improve the sodium wetting[8–13]. In Run 1-5 to 1-8, the residual sodium amounts on the 7-pin assembly were quantitatively measured to evaluate both the amounts of the sodium film deposited on the pin surface and the sodium lump at the bottom of the pins. The withdrawal speeds of Run 1-5 and 1-7 were the same as Run 1-1 and 1-3. They were 0.004 ± 0.000 m/s in Run 1-5 and 1-7. Those of Run 1-6 and 1-8 were the same as Run 1-2 and 1-4. They were 0.202 ± 0.052 m/s in Run 1-6 and 0.189 ± 0.017 m/s in Run 1-8. Comparing the residual sodium amounts of the single pin and 7-pin assembly of the same withdrawal speed, the amount of the sodium lump at the assembly was evaluated. It occurs due to the narrow gaps between the pins. The temperature conditions in Run 1-7 and 1-8 are the same as Run 1-3 and 1-4. The liquid sodium of 350°C could improve the sodium wetting of the pin surface. According to the Longson experiments[12], the

sodium wetting of type-316 stainless steel was improved at 400°C in one hour. According to the Yoshida experiments[13], the sodium wetting of type-304 stainless steel improved above 380°C for the short time. We measured a series of Run 1-1 to 1-11 three times to evaluate the average values and the standard errors (SE) of the mean of the residual sodium amounts and the withdrawal speeds. Here, the standard error of mean is given by $\sigma/\sqrt{n}$. The σ is the standard deviation, and the n is the number of the tests conducted ($n = 3$).

< Table 2 >

III. Estimation method

The residual sodium in the dummy fuel assembly can be divided roughly by the sodium deposited on the fuel pin surface (m_{Dummy}) and the sodium deposited on the structures in a hexagonal wrapper tube (M_{Dummy}). Fortunately, we have a lot of proven track records for the Monju driver fuel assembly, in which the residual sodium amounts ($M_{Driver} + m_{Driver}$) have been measured repeatedly[3]. The M_{Dummy} can be estimated approximately from the residual sodium amount of the Monju driver fuel assembly ($M_{Driver} + m_{Driver}$) and the residual sodium amount on the single-pin surface (m_{Single}): $M_{Dummy} \approx (M_{Driver} + m_{Driver}) - 169 \times m_{Single}$. Here, 169 is the pin number. This is because only the thin sodium film remains on the Monju driver fuel pins due to the wire spacer. Therefore, we can evaluate the $M_{Dummy} + m_{Dummy}$ by using the m_{Single} (for single pin) and the m_{Dummy} (for 169 pins). This paper focuses on the residual sodium amount of the dummy fuel pins such as amounts of the liquid sodium film and sodium lumps between the pins (m_{Single} and m_{Dummy}).

The estimation method was to combine the representative equations of a viscosity flow model, the LLD model, an empirical equation related to Bretherton model, and a capillary force model in a tube. The four calculation models treat the hydrodynamics and wetting phenomenon of solid interfaces: the first is a problem of a thinning film on a wet vertical plate in the III.A. section. The second is the

Landau-Levich-Derjaguin (LLD) model as a capillary forced problem in the III.B. section. The third is another geometry problem of a capillary tube which is applied by the LLD model in the III.C. section. The last is the balance of the gravitational force and capillary force in a capillary tube in the III.D. section. **Figure 4** depicts the outlines for these models.

< Figure 4 >

III.A. Viscosity flow model

The previous distinguished works considered a thin liquid film placed on a vertical base for this model[4 17]. This model is based on the liquid film flowing on the stationary vertical base, which is called the viscous flow regime. The liquid film is dominated by viscous forces and gravitational attraction. The reasons are that the layer is thin, the motion is nearly laminar flow, and the curvature of the liquid film can be ignored. The viscous force is given by the viscosity (η). The gravitational attraction is given by the liquid density (ρ) and the gravitational constant (g). The ratio of the withdrawal length and time is equal to the withdrawal speed (U_0) relatively. From this model, the maximum liquid film thickness (h_1^O) can be calculated by the following equation, which is well-known as the Jeffreys solution[17]. Here, the C_1 in Equation (1) is close to 0.8, which is related to the curvature of the dynamic meniscus.

$$h_1^O = C_1\sqrt{\frac{\eta U_0}{\rho g}} \tag{1}$$

The model was applied for the sodium film thickness deposited on the outer surface of the pins in Run 1-1, 1-3, 1-5, and 1-7 because of the slow withdrawal speed.

III.B. Landau-Levich-Derjaguin (LLD) model

Landau-Levich-Derjaguin (LLD) model is a modified form of the viscous flow of Equation (1)[4 18–20]. The viscosity flow model considers only the viscosity and gravitational force, but the LLD model includes the surface tension of liquid film around the pool surface. In the region, a capillary number ($Ca = \eta U_0/\gamma$) becomes a dominant parameter, which represents the ratio of the viscous drag forces versus the surface tension (γ). In the LLD model, the viscous force is equal to the capillary force around the pool surface, which derives the LLD film thickness equation.

$$h_2^O = C_2 Ca^{\frac{1}{6}} \sqrt{\frac{\eta U_0}{\rho g}} \qquad (2),$$

which can estimate the thickness of liquid film on the pin surface (h_2^O) at a wide range of withdrawal speeds. In the other past studies[6–7], the LLD model was applicable for the residual sodium amounts around the fuel pins, which means it is applicable for unloaded Monju dummy fuel assembly. Here, the C_2 in Equation (2) is close to 0.944, which was derived by numerical simulations[4 21–23].

The model was applied for the thickness of the residual sodium deposited on the outer surface of the pins in Run 1-2, 1-4, 1-6, 1-8, 1-9, 1-10, and 1-11 for the experiments of the more than 0.1 m/s withdrawal speed.

III.C. Empirical Equation Related to Bretherton Model

An empirical equation related to Bretherton model is a half-theoretical and half-empirical equation. It is applied for a capillary tube using the LLD model, leading to the formulation of the empirical equation. The empirical parameters were determined by the experimental data of the various liquids[24–25]. When the gravitational and inertial forces are negligible for a liquid in a capillary tube, the liquid film thickness (h_1^I) is deposited on the inner wall of a tube (tube radius: b) by the competition between viscous and capillary forces. It depends on the capillary

number. The h_1^I in the tube has been predicted by Bretherton law for $Ca \ll 1$, $h_1^I/b = 1.34Ca^{2/3}$. Recently, it is known that the h_1^I in the tube has been calculated by the following empirical equation through experiments[4 24–25].

$$h_1^I = b\frac{1.34Ca^{2/3}}{1+2.5\cdot 1.34Ca^{2/3}} \quad (3)$$

Here, the U_0 in C_a is a draining speed of liquid in Figure 4. In the paper, the U_0 is taken as a withdrawal speed of the tube relatively. The model was applied for the narrow gap surrounded by the three pins in Figure 1. The b was the equivalent radius for the area of the gap surrounded by the three pins.

III.D. Capillary force model in tube

The sodium lump (height: L) occurs at a bottom gap between the pins, where the shape of the meniscus is determined by the balance of the capillary force and gravitational force. The capillary forces are given by the surface tension (γ), the receding, and advancing contact angles (θ_r and θ_a)[4 24–25]. The gravitational force is given by the liquid density and the gravitational constant. The L is estimated by the following equation.

$$\frac{2\gamma}{b}(cos\theta_r - cos\theta_a) = \rho gL \quad (4)$$

Here, the b is the equivalent radius for the area of the gap surrounded by the three pins. According to Longson's experiments[12] and Kudoh's discussion[6–7], the receding and advancing contact angles of liquid sodium on the stainless steel were $\theta_r \approx 34°$ and $\theta_a \approx 90°$ at more than 400°C and the static contact angle is $51°$ at 280°C. The angles depend on the temperature and the immersion time. Because the receding contact angle is smaller than the static contact angle generally, this paper uses $\theta_r \approx 34°$ and $\theta_a \approx 90°$ under the condition of preheating at 350°C for two hours and $\theta_r \approx 51°$ and $\theta_a \approx 90°$ under the 200°C condition, respectively.

III.E. Physical parameters

Table 3 shows the equivalent radius (b) of the gap surrounded by the three pins and the physical parameters of liquid sodium at 200°C[26]. The viscosity (η), density (ρ), and surface tension (γ) of liquid sodium at 200°C were 4.519×10^{-4} (Pa s), 903.6 (kg/m^3), and 0.187 (N/m) [26], respectively.

< Table 3 >

III.F. Estimation method

Figure 5 shows the estimation method to combine the four calculation models represented by Equations (1)–(4). Equations (1) or (2) were applied for the sodium film thickness of the outer surface ($h_0^O = h_1^O$ or h_2^O). The length of the pins was L_0. The circumference of the pin was $A = 2\pi b$. Equation (3) was applied for the narrow gap surrounded by the pins. The equivalent radius of the gap was b. The length was $L_0 - L$. Equation (4) was applied for the sodium lump at the bottom gap between the pins. The area was $S = \pi b^2$. The length was L.

We calculated the sodium film thickness of the outer surface ($h_0^O = h_1^O$ or h_2^O) and inner surface (h_1^I) of the pins and the sodium lump height (L) deposited on the unloaded pins using Tables 2 and 3. In the numerical calculation, the h_0^O and h_1^I were determined by using the withdrawal speed (U_0), which was evaluated by the image analysis in the experiment, and the physical properties of sodium at Table 3. The L was determined by the contact angles (θ_r and θ_a), which depended on the temperature, and the gravitational force of sodium lump. Finally, we estimated the residual sodium amount on the dummy fuel pins (m) by the following equation:

$$m = 22\rho A h_0^O L_0 + 294[\rho A h_1^I (L_0 - L) + \rho S L] \qquad (5)$$

Here, the 22 and 294 are the equivalent quantity of the pin for the outer surface facing the wrapper tube and for the inner surface facing the gap.

< Figure 5 >

IV. Results and discussion

Through all tests, we have observed a common physical phenomenon: when the test specimen was extracted, the liquid sodium covered the surface of the test specimen. The covering sodium was seemed to be a liquid phase for more than 10 minutes due to the large heat capacity of the test specimen. As time passed, the stainless-steel surface of the test specimen could be visualized. Furthermore, the liquid sodium was solidified as it was, except for Run 1-9–1-11 and 2-1–2-3. Therefore, the waiting time for the sodium solidification on the test specimen didn't influence the measured values of the residual sodium amounts. The residual sodium amounts didn't change at all after extracting the pins in Run 1-1–1-8. However, in Run 1-9–1-11 of the 169-pin test specimen, we sometimes observed that several sodium droplets fell due to the accumulation of liquid sodium. It terminated with the vibration of the test specimen.

To quantitate the sodium amounts deposited on the pins, **Table 4** shows the sodium concentration (g/cc) in the blank industrial alcohol and the post-test chemical analysis sample of the rinsed alcohol solution. We obtained the residual sodium amounts at the tests from the sodium concentration and the amounts of the rinsed solution.

< Table 4 >

IV.A. Residual Sodium Amounts on Surface of Single Pin

The blue bar graphs in **Figure 6** depict the average amounts of the residual sodium obtained by the single pin experiments. The orange bar graphs in Figure 6 depict those of the calculation results with Equation (1) for Run 1-1 and 1-3 and Equation (2) for Run 1-2 and 1-4. The error bars denote the standard errors of mean in three times experiments and in calculation results using the three different withdrawal speeds obtained from the image analyses, respectively. Figure 6 clearly

shows the reasonable dependence of the experimental conditions such as the withdrawal speeds and the sodium wetting. Comparing Run 1-1 and 1-2 and/or Run 1-3 and 1-4, the residual sodium amounts increased as the withdrawal speed increased. In Run 1-3 and 1-4, the residual sodium amounts were much larger than those in Run 1-1 and 1-2 due to the improvement of the sodium wetting. Especially, it was remarkable in Run 1-4. This denotes that improvement of the sodium wetting increases drastically the amounts of the residual sodium.

< Figure 6 >

The calculation results using Equations (1) and (2) show the same amounts of residual sodium as the experiments except for Run 1-4. The LLD model includes the capillary force, but the calculation results in Run 1-4 show much smaller values than the experimental results. We regarded it as the difference of the sodium wetting, which would mean the difference of the adhesion energy. Namely, because the adhesion energy increased by preheating and improving the sodium wetting, the residual sodium amounts were considered to increase in Run 1-4. The classical adhesion energy, $\gamma_{SO} - \gamma_{SL} = \gamma cos\theta_E$, is calculated by the Yang-Dupré equation. Here, γ_{SO} and γ_{SL} are a solid-gas and solid-liquid interface energy, respectively. The ratio of the adhesion energy ($\gamma_{SO} - \gamma_{SL}$) should be determined by the static contact angle (θ_E). For simplicity, the static contact angle is defined as the average of the receding and advancing contact angles: $\theta_E = (\theta_r + \theta_a)/2$. In the residual sodium, the ratio of the adhesion energy is calculated as $\cos(34° + 90°)/\cos(51° + 90°) \approx 1.4$. The grey bar graphs in Figure 6 depict 1.4 times the estimation values of the LLD model. The calculation result in Run 1-4 showed closer to the experimental result.

Figure 7 shows the appearance of the unloaded single pin for Run 1-1 and Run 1-3. The liquid sodium on the pin surface was attached partially and solidified like a splash pattern because of fluid instability. The residual sodium on the pin surface in Run 1-3 was seemed more enormously.

< Figure 7 >

IV.B. Formation of Sodium Lump at Bottom of 7-pin Assembly

The blue bar graphs in **Figure 8** depict the average amounts of the residual sodium obtained by the 7-pin assembly tests in Run 1-5 to 1-8. The orange bar graphs in Figure 8 depict those of the calculation results using Equations (1), (3), and (4) for Run 1-5 and 1-7 and Equations (2), (3), and (4) for Run 1-6 and 1-8. The grey bar graphs in Figure 8 depict the sodium amounts of 1.4 times the estimation values of the LLD model. In Run 1-5 to 1-8, the orange bar graphs obtained by the calculation are smaller than the blue bar graphs of the experiments, but the grey bar graphs in Run 1-7 and 1-8 became closer to the experiments. **Figure 9** depicts the categories of the residual sodium amounts in Run 1-5 to 1-8, which were obtained by the calculation. The grey, blue, and orange bar graphs represent the amounts of the sodium lump at the bottom of the pins, the sodium film on the inner, and outer surface of the pins, respectively. Here, the inner surface of the pins means the pin surface surrounded by the other pins, and the outer surface of the pins means the pin surface that isn't surrounded. The amounts of the sodium lump were independent of the withdrawal speed, but they were related strongly to the sodium wetting. The heights of the sodium lumps are in an agreement between the calculation results and experimental observation: in the calculation, the heights were approximately 27 mm in Run 1-5 to 1-6 and 35 mm in Run 1-7 to 1-8. In experimental findings, the heights of the sodium lumps were 28–33 mm with a visual inspection. Furthermore, the amounts of the sodium films on the inner surface were relatively lower than the sodium amounts of the outer surface and those of the sodium lump, because the gap was a very small width (~0.1 mm). The amounts of the sodium films on the inner and/or outer surface trended to increase slightly as the withdrawal speed increased. By increasing the withdrawal speed from 0.004 m/s to more than 0.1 m/s, the amounts of the sodium films on the inner and outer surfaces increased more than double.

< Figure 8 >

< Figure 9 >

Figure 10 depicts the dependence between the withdrawal speed and thickness of sodium film on the outer/inner surface of the unloaded pin. The orange, blue, and grey lines show the calculation results of the viscosity flow model of Equation (1), the LLD model of Equation (2), and the empirical equation of Equation (3), respectively. The vertical and horizontal axes of Figure 10 represent the thickness of the sodium film on the pin surface and the withdrawal speed, respectively. The viscosity flow model gave us the largest values of all, but the viscosity flow model couldn't apply for only small withdrawal speed conditions. Therefore, we draw the dashed orange line over 0.01 m/s. The LLD model is a useful model for a wide range of withdrawal speed. It can estimate at less than several tens of micrometres in film thickness. In Kudoh's assessments for the residual sodium amounts on the fuel assembly, the LLD model was used[6–7]. The empirical equation related to the Bretherton model gave us the sodium film thickness on the inner surface of the pins. The thickness is less than 10% of that on the outer surface of the pins obtained by the LLD model. Therefore, it concluded that the total amounts of the residual sodium are strongly affected by the sodium lumps at the bottom of the pins.

< Figure 10 >

Figure 11 depicts the dependence of the residual sodium amount on the number of pins. We added and placed the pins at one layer of hexagons around the centre pin: the number of pins was taken as 1, 7, 19, 37, 61, 91, 127, and 169. The green, orange, and grey bar graphs show the amounts of the sodium film on the outer surface of pins using Equation (2), those of the sodium film on the inner surface of pins using Equation (3), and those of sodium lump using Equation (4), respectively. The numeral of each bar graph denotes the sodium amount (gram) obtained by the calculations. When the number of pins was small, the amounts of the sodium lump were comparable to the sum of the others. As the number of pins increased, the total amounts of the residual sodium increased linearly. The amounts of the sodium lump became dominant. It accounted for more than 79% of the total amount of residual sodium in 169 pins. If we need to consider a method which decreases the residual sodium amounts in the dummy fuel assembly, a dry cleaning

method[6–7] such as Ar gas blowing might be one of the effective methods, because the sodium lumps clog the gaps between the pins.

< Figure 11 >

IV.C. Estimation for Amounts of the Residual Sodium at 169-pin Assembly

Figure 12 depicts the amounts of the residual sodium on the unloaded 169-pin assembly in Run 1-9 to 1-11. The blue bar graphs in Figure 12 show the amounts of residual sodium obtained by the experiments. The measured values were 30.6 g, 21.8 g, and 28.0 g. The experimental value in Run 1-10 was lower than in Run 1-9 and 1-11 because some horizontal oscillations of the 169-pin assembly were observed during extracting the test specimen. Several sodium droplets fell. It terminated with the vibration of the test specimen. The average value is 26.8 g, and the standard errors are 2.6 g in Run 1-9 to 1-11. The rightmost bar graph in Figure 12 shows the amounts of the residual sodium, which were estimated by using Equation (5) with $U_0 = 0.1$ m/s. The estimated value of 28.2 g shows close to the average of the experimental data. This calculation gives us a good estimation value for the amounts of residual sodium on the unloaded dummy fuel pins. Furthermore, the calculation can predict the deposited place of the residual sodium. The amount of sodium lump at the bottom of the pins accounts for much larger than the others, such as sodium films on the outer/inner surface of the pins. The ratio reaches close to 79% of total residual sodium amounts. It concluded that we could estimate the amounts of the residual sodium attached on the unloaded Monju dummy fuel assembly by using Equation (5). However, we should note that the effects of sodium wetting have the potential to change drastically the amounts of the residual sodium. When the sodium wetting effect needs to be considered in the estimation, we should multiply the amounts of the sodium films on the outer/inner pin surface with 1.4.

< Figure 12 >

IV.D. Demonstration of sodium draining behavior through 169-pin Assembly

Figure 13 shows the examples of (a) the 169-pin assembly with a wrapper tube immersed in the sodium pool and that of (b) the 169-pin assembly with a wrapper tube unloaded from the sodium tank in Run 2-1 to 2-3. Figure 13 demonstrates directly the sodium draining behaviors through the dummy fuel assembly. Prior to extracting the test specimen from the sodium pool, we immersed the test specimen in the sodium tank, and the cover gas was evacuated by a pump to replace the gas with liquid sodium. The inner part of the wrapper tube of the test specimen and the gap between the 169 pins were filled with liquid sodium. We conducted three times withdrawal tests of the 169-pin assembly with a wrapper tube from the sodium pool (Run 2-1 to 2-3). When the 169-pin assembly was extracted, the sodium seemed to maintain in the wrapper tube for several 0.1 seconds. Then, liquid sodium in the wrapper tube fell through the drain ports. Because the drain port was designed as a small size such as approximately $30\text{mm}^{\text{H}} \times 20\text{mm}^{\text{L}} \times 30\text{mm}^{\text{W}}$, the liquid sodium was considered to maintain in a slight time. Figure 13 (b) shows the unloaded specimen. We have never observed that much amount of sodium remained at the top of the pins. The sodium draining behavior showed high reproducibility in our tests. Therefore, it concluded that the liquid sodium in the Monju dummy fuel assembly can drain by the withdrawal. Because the liquid sodium drains through the gaps between the pins, the amount of the residual sodium deposited on the dummy fuel pins can be evaluated with Equation (5).

< Figure 13 >

IV.E. Uncertainty Analysis of Estimation Method

Figure 14 shows the results of the uncertain analysis for the residual sodium amounts. The vertical axis is the experimental values, and the horizontal axis is the calculation values obtained in this study. The solid line shows the straight line represented by $y = x$. Therefore, when the calculation values are completely equal to the experimental values, the data are placed on the solid line.

The dashed lines show the straight lines represented by $y = 1.63x$ and $y = 0.6x$. The experimental and calculation data in Figure 14 were placed at the inside of the two dashed lines. Therefore, the uncertainty of the residual sodium amount on the pins using Equation (5) was estimated at -40% to +63%. The errors are not relatively small values because the improvement of the sodium wetting and the withdrawal speed affected the residual sodium amounts. To address the sodium wetting phenomena, we need to research the complex interaction between liquid sodium and stainless steel extensively. However, this study can contribute to the assessment of the residual sodium amounts of the Monju dummy fuel assembly, because the estimation values were -23% to +9% in the experimental values in Run 2-1 to 2-3. These tests are the closest experimental conditions to Monju. They are except for improving the sodium wetting and changing the withdrawal speed intentionally.

< Figure 14>

V. Conclusions

In this study, the estimation method for the amounts of the residual sodium film on the surface of the dummy fuel pins and the sodium lumps at the bottom of the dummy fuel pins has been researched by the experiments and the calculation. The estimation method focused on the amount of residual sodium on the dummy fuel pins without wire spacers. Based on the characteristics of the residual sodium on the dummy fuel pin, such as the thin sodium film at the upper of the fuel pin and the sodium lump at the bottom of the fuel pin, the estimation method was to combine the representative equations such as the viscosity flow model, the LLD model, the empirical equation related to Bretherton model, and the capillary force model in the tube.

The experiments revealed that the amounts of the residual sodium increased drastically by the withdrawal speed and the improvement of the sodium wetting. Furthermore, the tests using the 169-pin assembly gave us the practical amounts of

the residual sodium in the Monju dummy fuel assembly and demonstrated directly the sodium draining behavior through the gap between the dummy fuel pins.

The calculation results using Equation (5) showed close to the value for the residual sodium amounts obtained by the experiments: the residual sodium amounts increase with the withdrawal speed. The amounts of sodium lumps account for much larger than the others. The uncertainty of Equation (5) is within -40% to +63%. In Run 2-1 to 2-3, it is within -23% to +9%. This estimation method can contribute to the assessment of the residual sodium amounts on the unloaded Monju dummy fuel assembly.

Nomenclature

A	Circumference of pin
b	Equivalent radius of gap surrounded by three pins
Ca	Capillary number of liquid sodium at 200°C
C_1	Constant number
C_2	Constant number
g	Gravitational constant
h_1^I	Thickness of liquid sodium film by empirical equation on Bretherton model
h_1^O	Thickness of liquid sodium film by viscosity flow model
h_2^O	Thickness of liquid sodium film by LLD model
L_0	Height of pin
L	Height of sodium lump
m_i	Residual sodium amount on the pin surface (i: single fuel pin, driver fuel pin, and dummy fuel pin)

M_i Residual sodium amount on the assembly structure (i: driver fuel assembly and dummy fuel assembly)

n Number of the tests conducted

S Area of gap surrounded by three pins

U_0 Withdrawal speed of test piece

(Greek letters)

γ Surface tension of liquid sodium

γ_{SO} Solid-gas interface energy

γ_{SL} Solid-liquid interface energy

η Viscosity of liquid sodium

θ_a Advancing contact angle

θ_E Static contact angle

θ_r Receding contact angle

ρ Density of liquid sodium

References

1 Power Reactor and Nuclear Fuel Development Corporation, *Kousokuzoushokuro Monju Hatsudensho Genshiro Secchikyokashinseisho*, Chap. 8, p.8-8-14–8-8-27, Power Reactor and Nuclear Fuel Development Corporation, Tsuruga, Fukui (1980). [in Japanese]

2 F. NAKASHIMA, et al., "Prototype Fast Breeder Reactor Monju – Its History and Achievements –," JAEA-Technology 2019-007, p. 59, Japan Atomic Energy Agency (Jul. 2019).

3 Nuclear Regulation Authority; https://www.nsr.go.jp/data/000377967.pdf (current as of Jul. 13, 2022).

4 P. G. DE GENNES, F. BROCHARD-WYART, D. QUERE, *Gouttes, bulles, perles et ondes*, Part 2, Chap. 3–5, p. 67–135, Yoshioka Shoten Publishing, Kyoto, Kyoto (2003). [in Japanese]
5 C. J. BRINKER, *Chemical Solution Deposition of Functional Oxide Thin Films*, Chap. 3, p. 233–261, Springer Vienna, Vienna, Austria (2013).
6 H. KUDOH, et al., "Development of the Residual Sodium Quantification Method for a Fuel Assembly of SFRs," *J. Nucl. Sci. Technol.*, **57**, *4*, 9–23 (2020); https://doi.org/10.1080/00223131.2019.1691069.
7 H. KUDOH, et al., "Development of the Residual Sodium Quantification Method for a Fuel Pin Bundle of SFRs before and Dry Cleaning," *J. Nucl. Sci. Technol.*, **57**, *4*, 408–420 (2019); https://doi.org/10.1080/00223131.2019.1691069.
8 J. SAITO, Y. KOBAYASHI, H. SHIBUTANI, "Wettability of Pure Metals with Liquid Sodium and Liquid Tin," *Mater. Trans.*, **62***, 10,* 1524–1532 (2021); https://doi.org/10.2320/matertrans.MT-M2021107.
9 J. SAITO, Y. KOBAYASHI, H. SHIBUTANI, "Wettability of Pure Metals with Liquid Sodium and Liquid Tin," *J. Japan. Inst. Met. Mater.*, **85**, *3*, 110–119 (2021); https://doi.org/10.2320/jinstmet.J2020042. [in Japanese]
10 M. KAWAGUCHI, A. TAGAWA, S. MIYAHARA, "Reactive Wetting of Metallic Plated Steels by Liquid Sodium," *J. Nucl. Sci. Technol.*, **48**, *4*, 499–503 (2012); https://doi.org/10.1080/18811248.2011.9711725.
11 M. KAWAGUCHI, H. HAMADA, "Reactive Wetting by Liquid Sodium on Thin Au Plating," *J. Nucl. Sci. Technol.*, **51**, *2*, 201–207 (2013); https://doi.org/10.1080/00223131.2013.854712.
12 B. LONGSON, J. PRESCOTT, "Some Experiment on the Wetting of Stainless Steel, Nickel and Iron in Liquid Sodium," *Proc. Int. Conf. Liquid Alkali Metals*, London, England, April 4–6, 1973, p.171–176, The British nuclear energy society (1973).
13 E. YOSHIDA, "Technical Report on Sodium Technology in the Field of Material Research –On the Material Corrosion and the Mechanical Strength in High Temperature Sodium–," JAEA–Review 2013–026, p. 17–18, Japan Atomic Energy Agency (Dec. 2013).14 https://www.jaea.go.jp/04/tsk/english/kenkyu/kenkyu-5.html

15 B. WELZ, M. SPERLING, *Atomic Absorption Spectrometry*, Third Ed., Chap. 10, p. 575–769, Wiley-VCH, Weinheim, Chichester (1999).
16 HITACHI HIGH-TECH SCIENCE CORPORATION, "*Analysis of calcium, potassium, magnesium, and sodium in wine (flame atomization)*," Technical Report AA No.170006 Atomic Absorption Spectrophotometer, p. 4 (2018). https://biz.hitachi-hightech.com/sinavi/asi_sitesearch?q=ZA3300&viewLanguage=en_US (current as of Mar. 23, 2023).
17 H. JEFFREYS, "The Draining of a Vertical Plate," *Math. Proc. Camb. Phil. Soc.*, **26**, *2*, 204–205 (1930); https://doi.org/10.1017/S0305004100015437.
18 L. LANDAU, B. LEVICH, "Dragging of a Liquid by a Moving Plate," *Acta Physicochemica U. R. S. S.*, **XVII**, *1–2*, 42–54 (1942).
19 B. DERJAGUIN, "On the Thickness of the Liquid Film Adhering to the Walls of a Vessel after Emptying," *Acta Physicochemica C. R. Acad. Sci. URSS.*, **39**, *11*, 134–137.
20 J. H. SNOEIJER, et al., "Thick Films of Viscous Fluid Coating a Plate Withdrawn from a Liquid Reservoir," *Phys. Rev. Let.*, **100**, 244502 (2008); https://doi.org/10.1103/PhysRevLett.100.244502.
21 R. EMMANUELLE, B. FRANCOIS, "Withdrawing a Solid from a Bath: How Much Liquid Is Coated?," *Adv. Colloid. Interface. Sci.*, **247**, 100–114 (2017); https://doi.org/10.1016/j.cis.2017.01.006.
22 G. PENG, et al., "Film Deposition and Transition on a Partially Wetting Plate in Dip Coating," *J. Fluid Mech.*, **791**, 358–383 (2016); https://doi.org/10.1017/jfm.2016.64.
23 G. MASAO, I. W. LENGGORO, "Probing a Dip-coated Layer of Organic Molecules by an Aerosol Nanoparticle Sensor with Sub-100 nm Resolution Based on Surface-enhanced Raman Scattering," *RSC Adv.*, **5**, 5158 (2014); https://doi.org/10.1039/C4RA03850A.
24 D.-H JEOG, et al., "Deposition of a Particle-laden Film on the Inner Wall of a Tube," *Phys. Rev. Fluid*, **5**, *11*, 114004 (2020); https://doi.org/10.1103/PhysRevFluids.5.114004.

25 P. AUSSILLOUS, D. QUERE, “Quick Deposition of a Fluid on the Wall of a Tube,” *Phys. Fluid.*, **12**, *10*, 2367–2371 (2000); https://doi.org/10.1063/1.1289396.
26 O. J. FOUST, *Sodium-NaK Engineering Handbook. Volume I. Sodium chemistry and physical properties*, Vol. 1, Chap. 1, p. 13–37, Gordon and Breach, Science Publishers, Inc., United States, (1972).

Acknowledgements

One of the authors (M. K.) expresses gratitude to Dr T. Yamaguchi, leader of sodium technology development group and colleagues at Japan Atomic Energy Agency’s Tsuruga Comprehensive Research and Development Center for various discussions.

Declaration of interest statement

The authors declare that they have no known competing financial interests or personal relationships that could have appeared to influence the work reported in this paper.

Table 1. Chemical compositions of the Monju dummy fuel pins

Element	Fe	Cr	Ni	Mn	Si	C	P	S
Percent	bal.	18.73	8.23	1.70	0.24	0.05	0.04	0.03

Table 2. Experimental conditions.

Test No	Specimen	Preheated temperature	Withdrawal speed $U_0 \pm$ SE (m/s) [1)]
Run 1-1	Single pin	200°C for 1h	0.004 ± 0.000
Run 1-2	Single pin	200°C for 1h	0.170 ± 0.013
Run 1-3	Single pin	350°C for 2h	0.004 ± 0.000
Run 1-4	Single pin	350°C for 2h	0.189 ± 0.003
Run 1-5	7-pin assembly	200°C for 1h	0.004 ± 0.000
Run 1-6	7-pin assembly	200°C for 1h	0.202 ± 0.052
Run 1-7	7-pin assembly	350°C for 2h	0.004 ± 0.000
Run 1-8	7-pin assembly	350°C for 2h	0.189 ± 0.017
Run 1-9	169-pin assembly	200°C for 1h	0.1 [2)]
Run 1-10	169-pin assembly	200°C for 1h	0.1 [2)]
Run 1-11	169-pin assembly	200°C for 1h	0.1 [2)]
Run 2-1	169-pin assembly	200°C for 1h	0.1 [2)]
Run 2-2	169-pin assembly	200°C for 1h	0.1 [2)]
Run 2-3	169-pin assembly	200°C for 1h	0.1 [2)]

[1)] U_0 and SE are the average and the standard errors of withdrawal speed three times.

[2)] $U_0 = 0.1$ in Run 1-9 to 1-11 and Run 2-1 to 2-3 is taken as the winch specification.

Table 3. Physical parameters for the calculations of Equations (1)–(5).

Physical parameter	Value
Equivalent radius of pin (m)	$b = 1.0 \times 10^{-3}$
Sodium viscosity at 200 °C (Pa s)	$\eta = 4.519 \times 10^{-4}$ [25]
Sodium density at 200 °C (kg/m^3)	$\rho = 903.6$[25]
Sodium surface tension at 200 °C (N/m)	$\gamma = 0.187$[25]

Table 4. Sodium concentrations in the blank industrial alcohol and the diluted rinsed alcohol solution.

Test No	Sodium concentration (g/cc) $\times 10^{-3}$
Blank	0.02
Run 1-1	0.20±0.02
Run 1-2	0.38±0.05
Run 1-3	0.21±0.02
Run 1-4	0.72±0.07
Run 1-5	4.34±0.20
Run 1-6	4.80±0.75
Run 1-7	4.68±1.36
Run 1-8	6.43±1.27
Run 1-9	5.75±0.74
Run 1-10	4.87±1.87
Run 1-11	7.90±0.42
Run 2-1	1.75
Run 2-2	1.25
Run 2-3	1.60

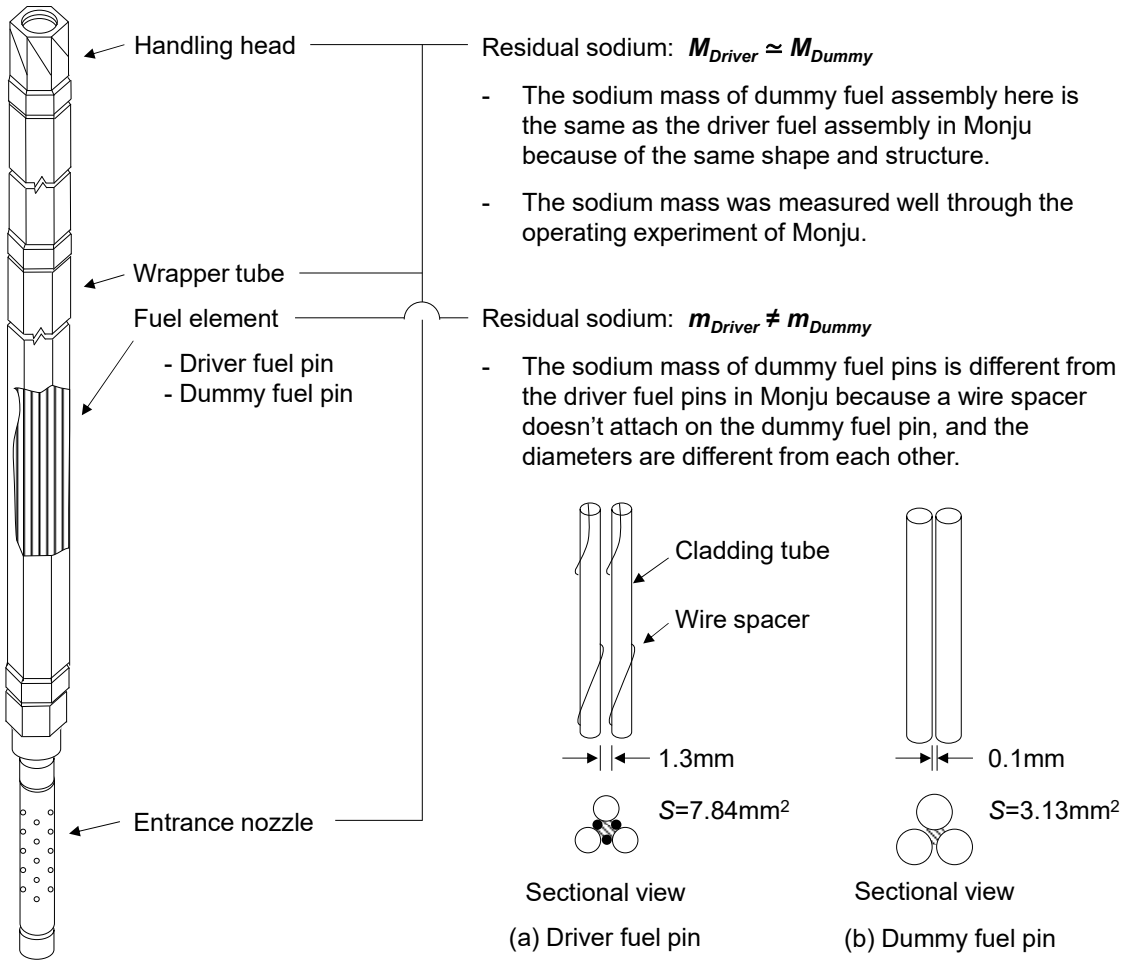

Figure 1. Sketch of a nuclear fuel assembly in Monju[2]. M_i and m_i (i=Driver fuel and Dummy fuel) denote the residual sodium mass on the driver and dummy fuel assemblies, respectively. (a) and (b) show outlines of the driver and dummy fuel pins. S is an area surrounded by the pins (hatched area).

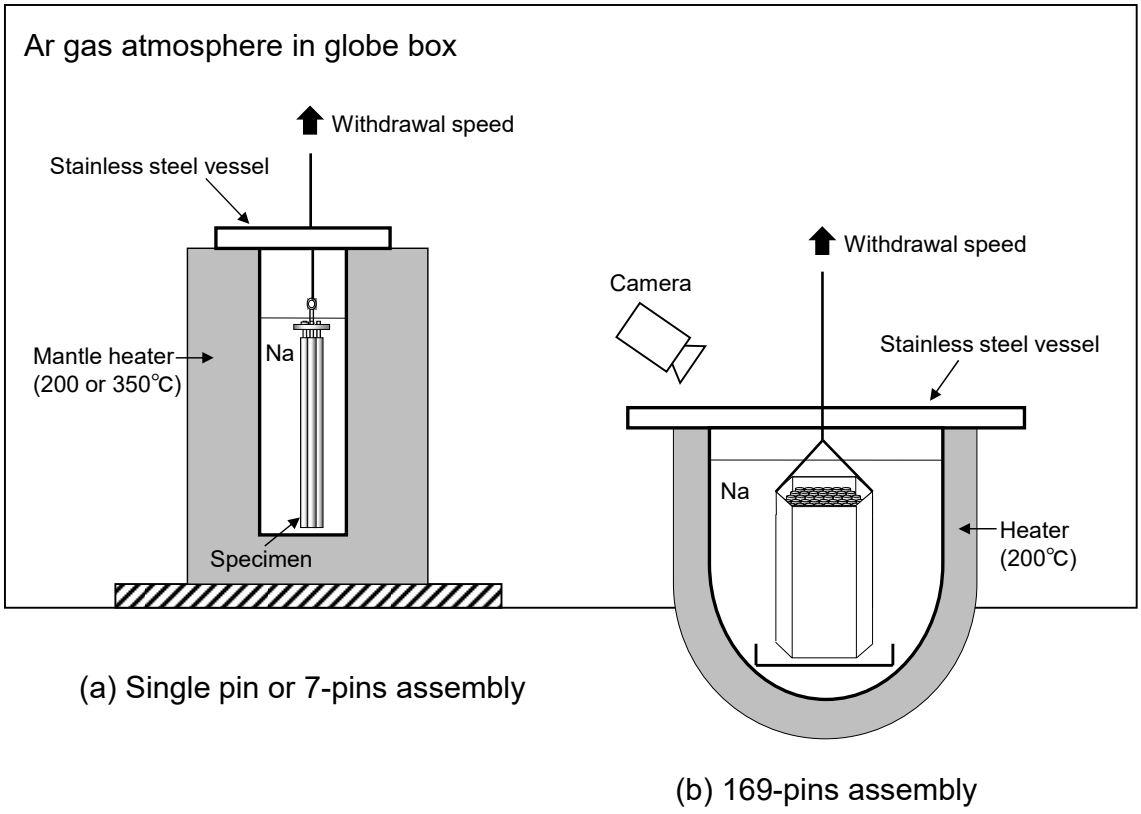

Figure 2. Overview of test apparatus for (a) Single pin or 7-pin assembly and (b) 169-pin assembly.

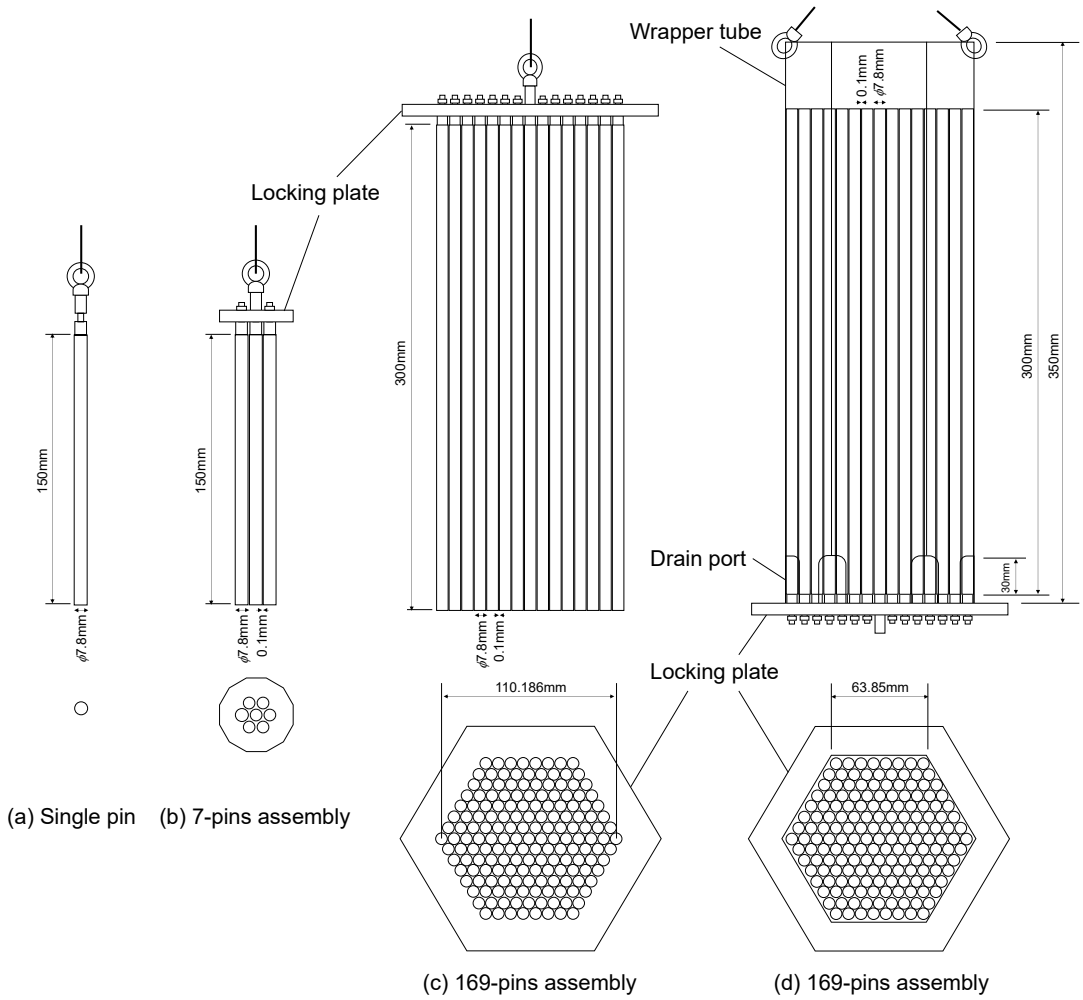

Figure 3. Test specimens of (a) Single pin, (b) 7-pin assembly and (c)–(d) 169-pin assembly.

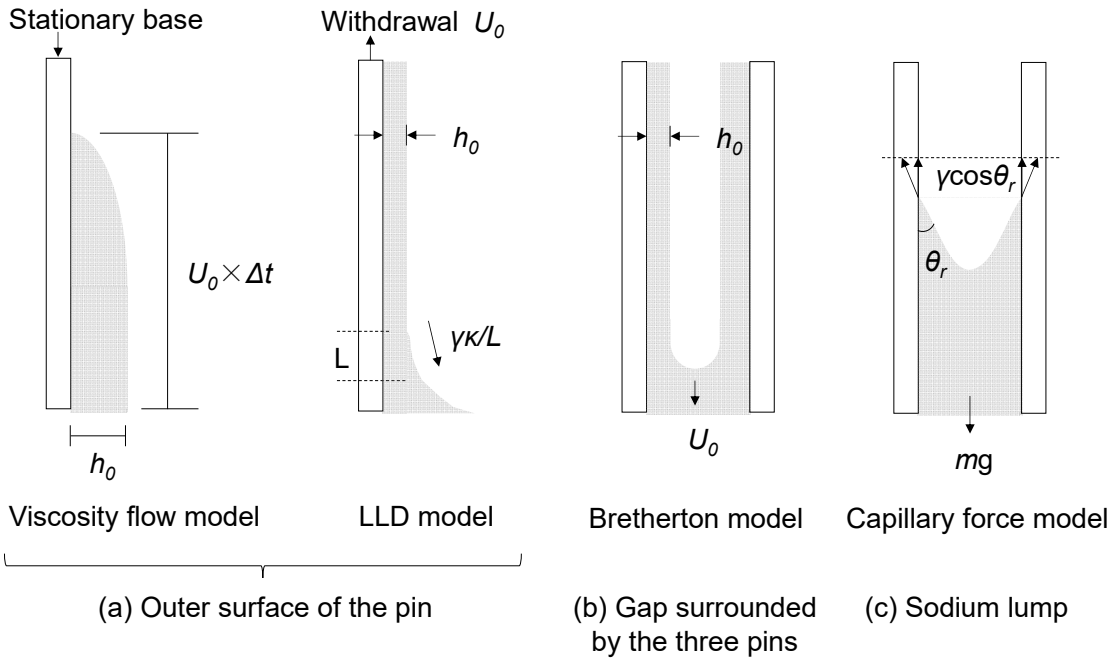

Figure 4. Outlines of four estimation models for residual liquid sodium on unloaded dummy fuel pins.

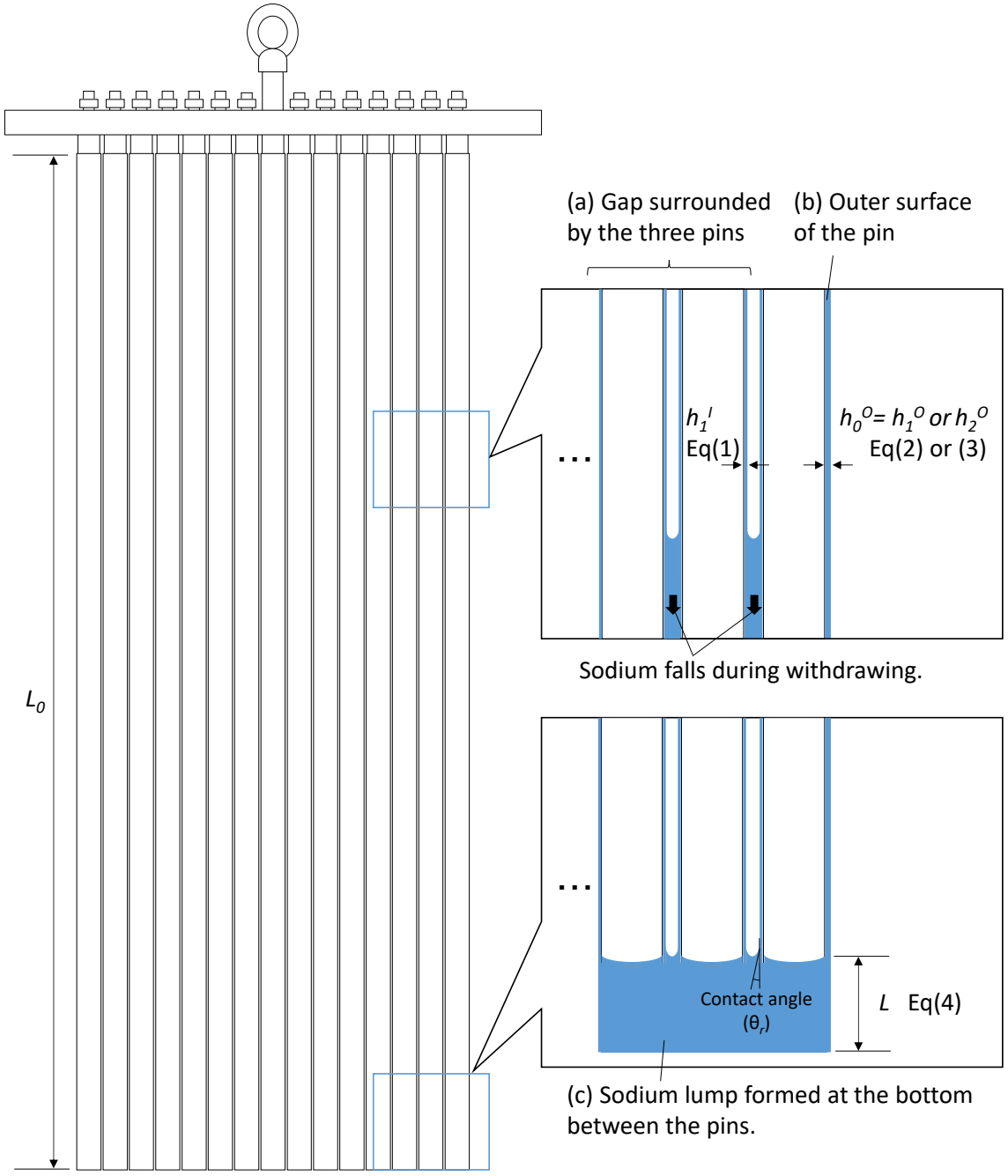

Figure 5. Characteristic sodium thin film on the pins and sodium lumps: their formation positions and estimation models in the estimation method.

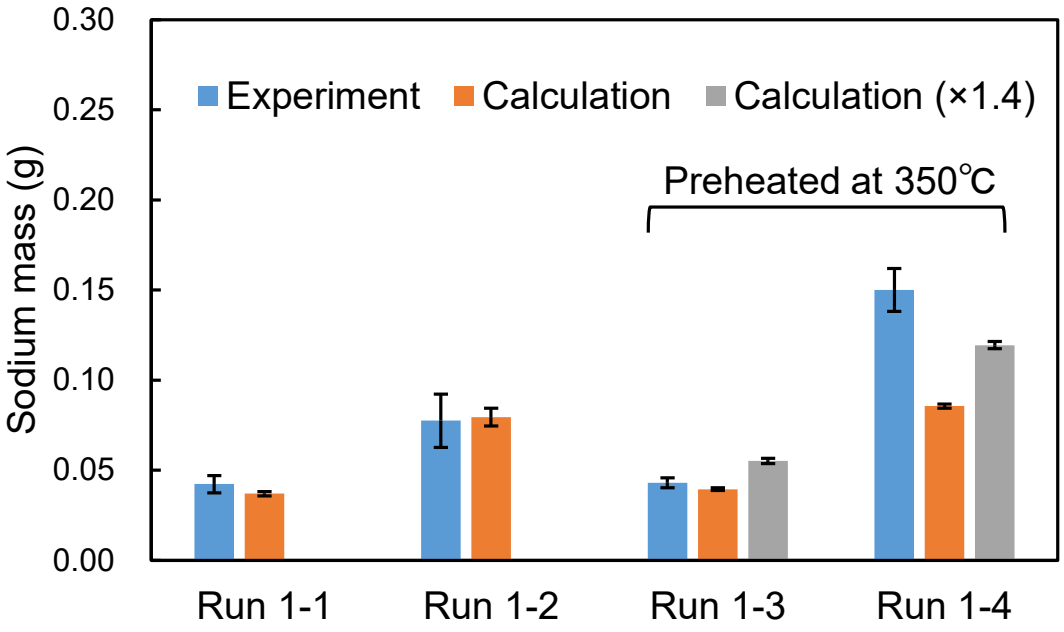

Figure 6. Residual sodium mass on an unloaded single pin which is obtained by experiments and calculations for Run 1-1 and 1-3 with Equation (1) and for Run 1-2 and 1-4 with Equation (2).

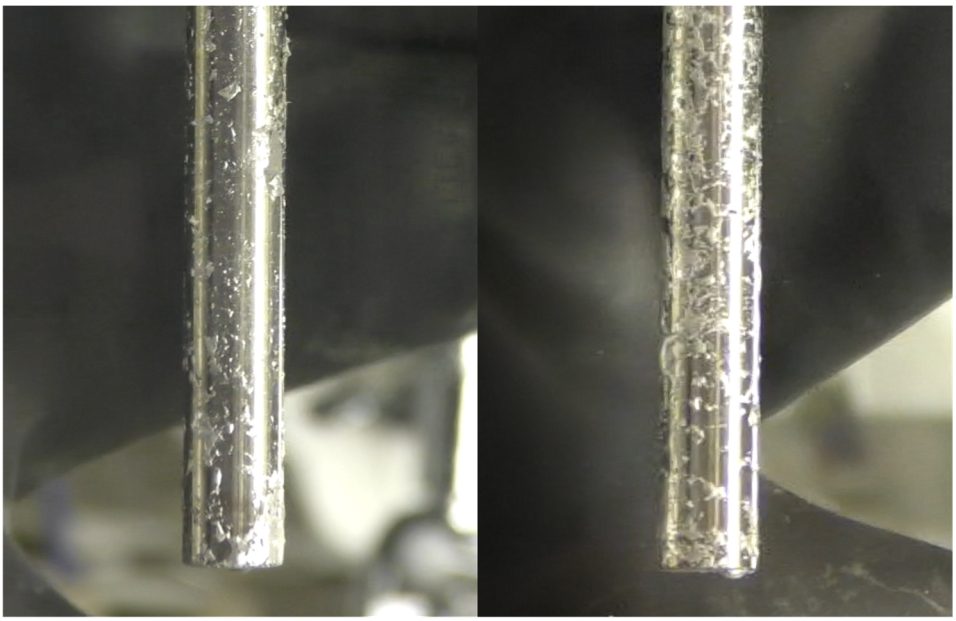

(a) Run 1-1: 200℃ (b) Run 1-3: 350℃

Figure 7. The appearance of residual sodium on the surface of the single pin in (a) Run 1-1 and in (b) Run 1-3.

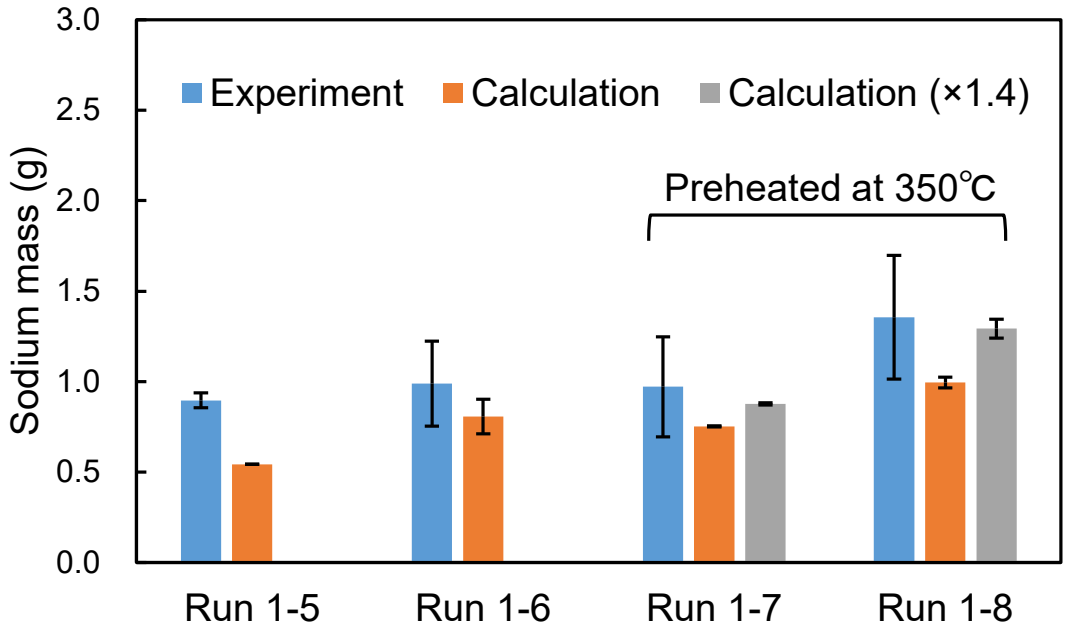

Figure 8. Residual sodium mass on unloaded 7-pin assembly which is obtained by experiments and calculations for Run 1-5 and 1-7 with Equations (1) and (3)–(4) and for Run 1-2 and 1-4 with Equations (2)–(4).

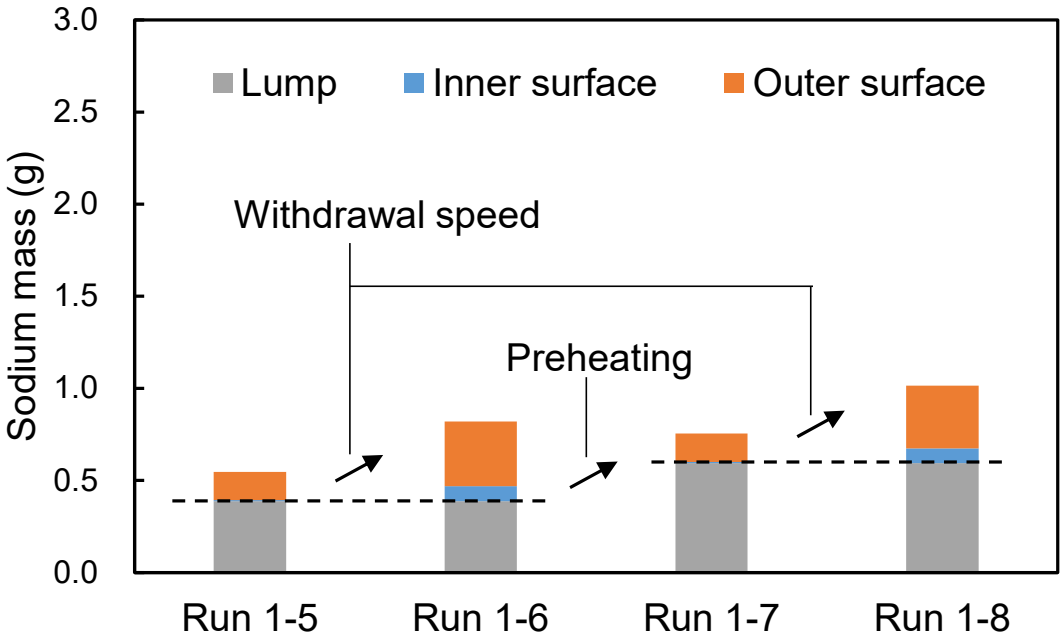

Figure 9. Estimated portions of residual sodium mass on unloaded dummy 7-pin assembly which are obtained by calculations.

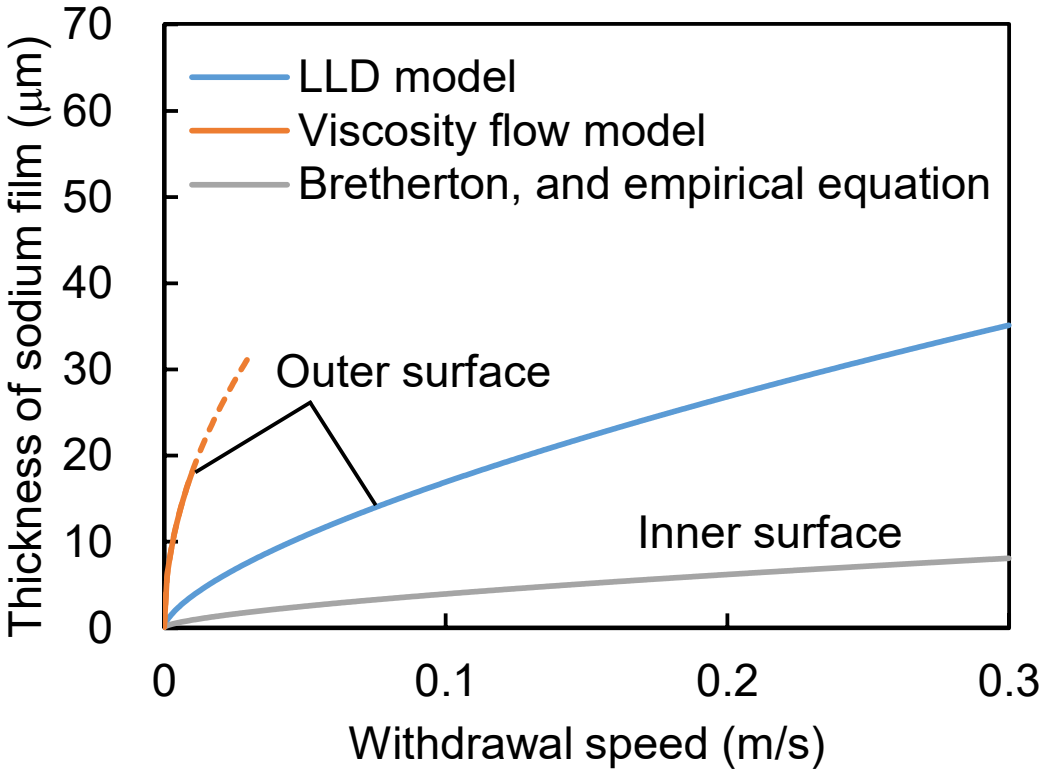

Figure 10. The thickness of sodium film on outer/inner surface of unloaded pin depending on withdrawal speed.

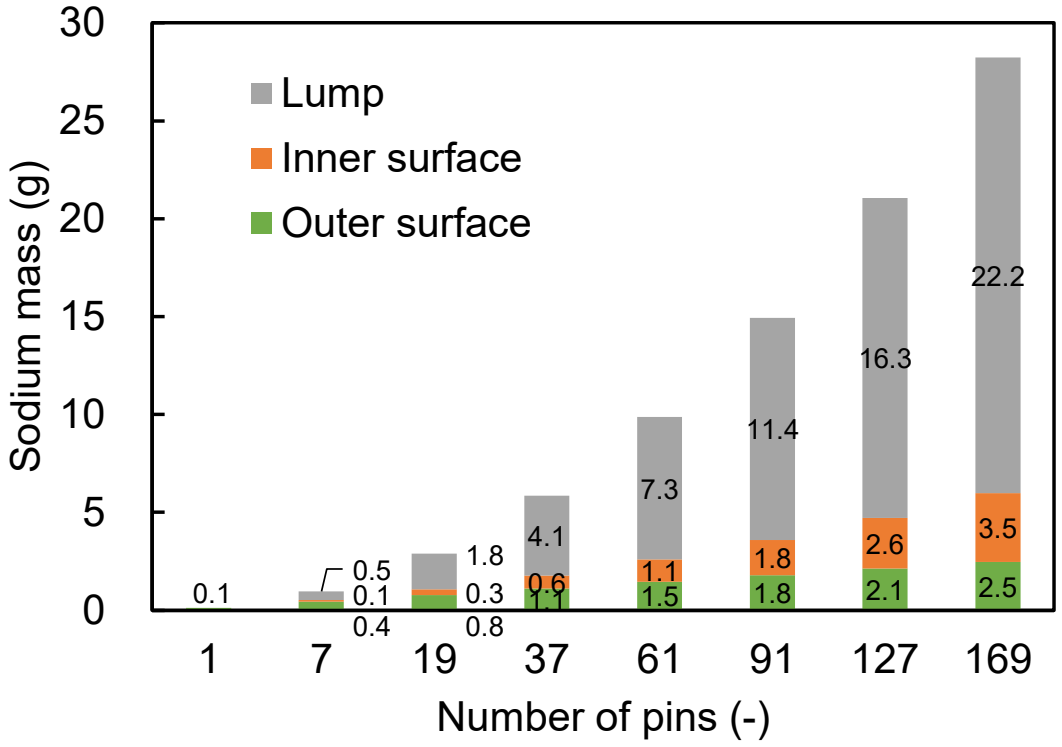

Figure 11. Dependence of residual sodium mass with number of dummy fuel pins.

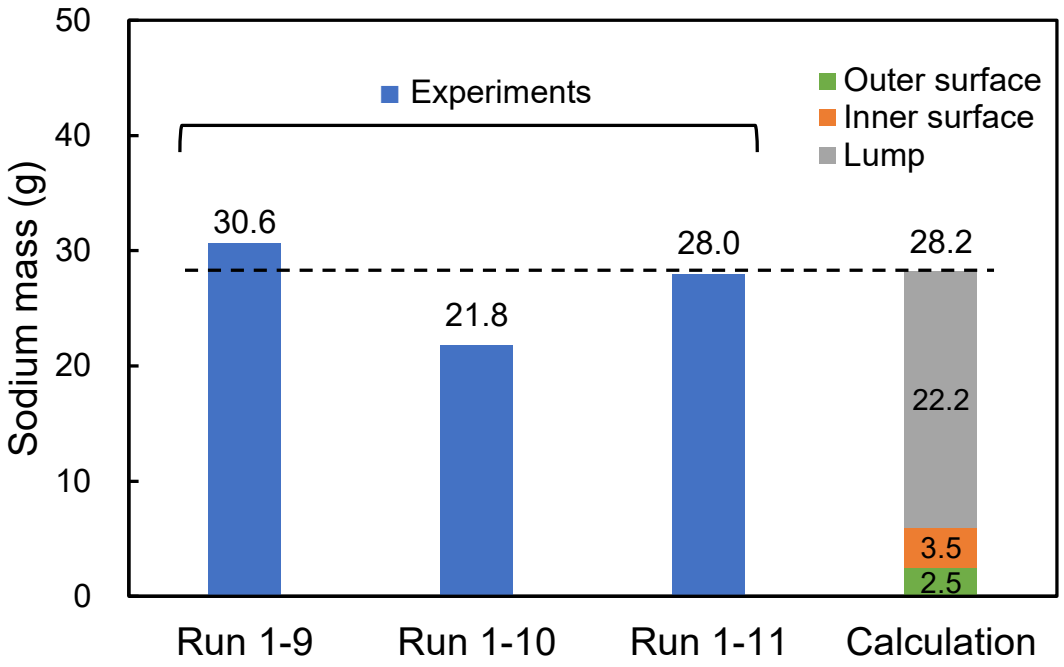

Figure 12. Residual sodium mass on unloaded 169-pin assembly.

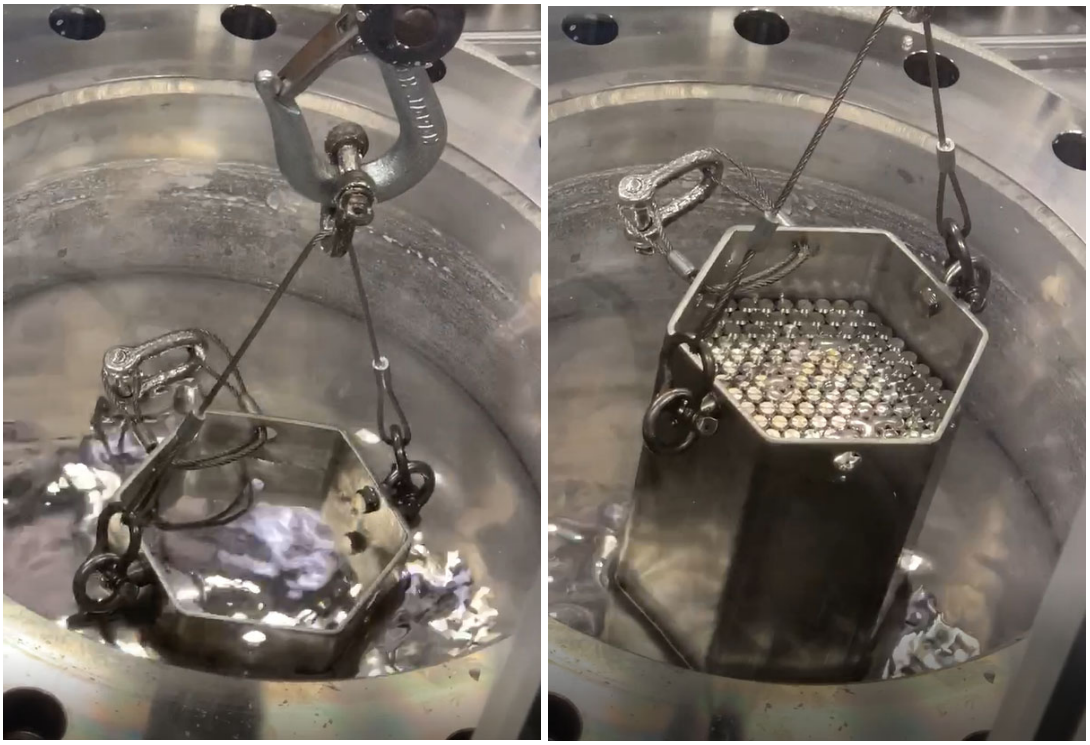

(a) In immersion (b) During withdrawal

Figure 13. Sodium draining behavior through 169-pin assembly with wrapper tube (a) in immersion of liquid sodium and (b) during extracting.

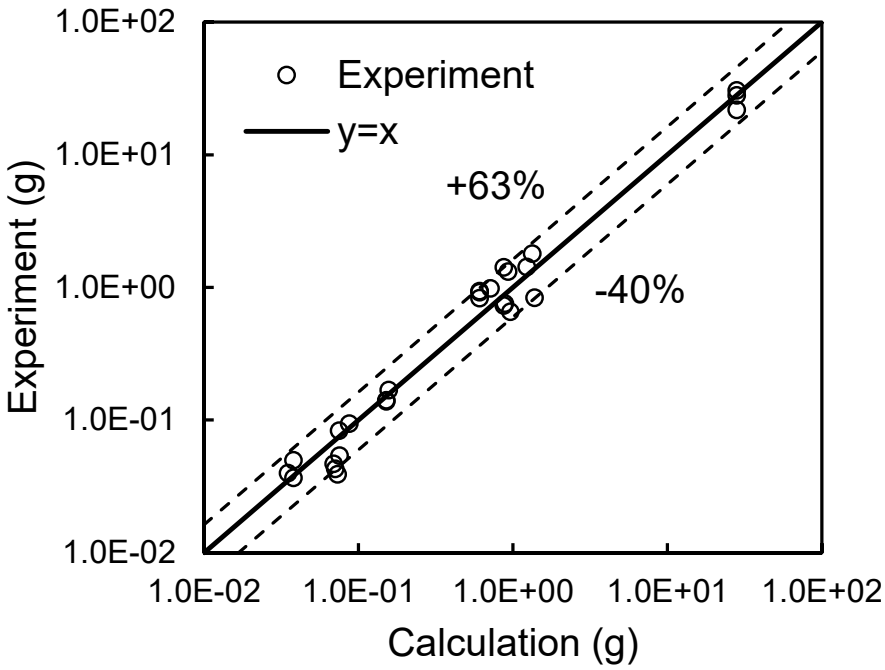

Figure 14. Uncertain analysis for the residual sodium amounts: the experimental values versus the calculation values in this study.